

Optimizing direct intense-field laser acceleration of ions

Zoltán Harman,^{1,2} Yousef I. Salamin,^{1,3} Benjamin J. Galow,¹ and Christoph H. Keitel¹

¹Max-Planck-Institut für Kernphysik, Saupfercheckweg 1, D-69117 Heidelberg, Germany

²ExtreMe Matter Institute EMMI, Planckstrasse 1, D-64291 Darmstadt, Germany

³Department of Physics, American University of Sharjah, POB 26666, Sharjah, United Arab Emirates

(Received 25 March 2011; published 7 November 2011)

The dynamics of ion acceleration in tightly focused laser beams is investigated in relativistic simulations. Studies are performed to find the optimal parameters which maximize the energy gain, beam quality, and flux. The exit ionic kinetic energy and its uncertainty are improved and the number of accelerated particles is increased by orders of magnitude over our earlier results, especially when working with a longer laser wavelength. Laser beams of powers of 0.1–10 petawatts and focused to subwavelength spot radii are shown to directly accelerate protons and bare nuclei of helium, carbon, and oxygen from a few to several hundred MeV/nucleon. Variation of the volume of the initial ionic ensemble, as well as the introduction of a pulse shape on the laser fields, have been investigated and are shown to influence the exit particle kinetic energies only slightly.

DOI: [10.1103/PhysRevA.84.053814](https://doi.org/10.1103/PhysRevA.84.053814)

PACS number(s): 37.20.+j, 42.65.–k, 52.75.Di

I. INTRODUCTION

In many important applications, charged entities, such as electrons, ions, and bare nuclei, need to be accelerated to specific energies, depending on the type of application in which they are employed. High-quality beams of charged particles find applications in medicine, industry, and fundamental research. Proton beams and beams of bare carbon nuclei are now either used or planned for utilization in the treatment of cancer [1–3]. Beams of highly charged ions, in addition to being used for radiotherapy, are candidates for near-future utilization in lithography [4]. Moreover, colliding beams of bare nuclei are used for studying the fundamental forces in nature and the production of heavy matter in the laboratory [5,6].

Besides acceleration to specific energies, these particles need to be produced in high-quality low-emittance beams. Such attributes are currently achievable using large and expensive conventional accelerators. Recently, high-quality proton beams have been produced by shining sub-picosecond high-intensity laser light onto thin-foil targets. This so-called target normal sheath acceleration (TNSA) is made possible by the strong quasistatic electric field created by the laser-accelerated electrons in a plasma [7]. Radiation pressure acceleration (RPA) may be an efficient mechanism at ultra-high intensities [8], or, by using circularly polarized pulses, at any intensity [9,10]. Recently, too, the direct acceleration of ions by means of counter-propagating variable-frequency pulses was investigated theoretically [11].

In this paper we present results of theoretical studies in which laser light is the source of energy to directly accelerate ions produced by other means. These particles gain substantial energy when subjected to present-day petawatt power laser systems, capable of generating electric fields several orders of magnitude stronger than the field of the proton at the site of the electron in a hydrogen atom (the atomic unit of electric field). The mechanism of acceleration is demonstrated and explained on the basis of the relativistic equations of motion of an ensemble of charged particles in strong laser fields. We investigate dependence of the accelerated particle beam properties, e.g., the exit kinetic energy distribution, the number of particles accelerated, on such laser system parameters as wavelength, power, and waist radius.

Our investigations result in an optimal range of parameters. We find that the number of accelerated ions can be increased by orders of magnitude compared to our earlier vacuum acceleration results [12] by increasing the laser wavelength by one order of magnitude. Furthermore, the energy gain of ions and its uncertainty are improved by increasing the wavelength of the laser field. This can be experimentally achieved, e.g., by using CO₂ lasers of a wavelength of 10.6 μm [13,14], rather than near-infrared lasers with wavelengths around 1 μm . Simulations in this paper demonstrate energy gains by protons and helium, carbon, and oxygen nuclei of up to several hundred MeV/nucleon as a result of interaction with linearly and radially polarized laser beams. These gains may be achieved even using a multiterawatt laser system, provided it is focused to a subwavelength waist radius. Focusing beams of multiterawatt or petawatt powers to μm spot sizes yields laser intensities of the order of 10^{20} – 10^{23} W/cm², which defines the range of interest. In radiotherapy, employing heavier ions, the required energies fall in the range 20–580 MeV/nucleon with less than 1% energy fluctuations [15].

Our paper is organized as follows. In Sec. II the linearly and radially polarized fields of a tightly focused laser beam will be briefly reviewed. Section III will be devoted to outlining the main single-particle equations and method of their solution, while the simulations will be described in Sec. IV. Simulations for acceleration of nuclei by linearly and radially polarized laser beams will be carried out and their results discussed in Secs. V and VI, respectively. In Sec. VII, effects of the size of the initial particle ensemble, and an added pulse-shape to the laser fields, on the kinetic energies of the accelerated particles, will be investigated and discussed. Our conclusions will be summarized in Sec. VIII.

II. THE FIELDS

In this section, fields of the laser beams will be briefly described. First of all, it should be recalled that the tightly focused beams develop axial as well as transverse electric and magnetic components. Tight focusing, to a waist radius $w_0 < \lambda$, also calls for a more accurate description of the fields beyond what is familiar from the paraxial approximation. The

corresponding laser power and intensity expressions ought also to be described to the same level of accuracy. For both linear and radial polarization, the parameters of a Gaussian beam will be used to model the fields. Those are the beam waist radius w_0 , the Rayleigh length (or depth of focus) $z_r = \pi w_0^2/\lambda$, where λ is the wavelength, and the diffraction angle $\varepsilon = w_0/z_r = \lambda/(\pi w_0)$.

A. Linear polarization

To save space in this paper, none of the field expressions will be quoted fully. Those expressions, giving the field components E_x, E_y, E_z, B_y , and B_z to order ε^{11} in the diffraction angle (defined above), may be found elsewhere [16]. We quote here only the leading couple of terms in each component, for the sake of the useful discussions to be presented below. With $O(\varepsilon^n)$ meaning the last term to be included in the component in question is of order ε^n , where $n = 10$ or 11 , the field components may be written as

$$E_x = E \left\{ S_1 + \varepsilon^2 \left[\xi^2 S_3 - \frac{\rho^4 S_4}{4} \right] + \dots + O(\varepsilon^{10}) \right\}, \quad (1)$$

$$E_y = E \xi \nu \{ \varepsilon^2 [S_3] + \dots + O(\varepsilon^{10}) \}, \quad (2)$$

$$E_z = E \xi \{ \varepsilon [C_2] + \dots + O(\varepsilon^{11}) \}, \quad (3)$$

$$B_x = 0, \quad (4)$$

$$B_y = \frac{E}{c} \left\{ S_1 + \varepsilon^2 \left[\frac{\rho^2 S_3}{2} - \frac{\rho^4 S_4}{4} \right] + \dots + O(\varepsilon^{10}) \right\}, \quad (5)$$

$$B_z = \frac{E}{c} \nu \{ \varepsilon [C_2] + \dots + O(\varepsilon^{11}) \}. \quad (6)$$

With ω the angular frequency of the fields, $\xi = x/w_0$, $\nu = y/w_0$, $\zeta = z/z_r$, $\psi_G = \tan^{-1} \zeta$, and $r = \sqrt{x^2 + y^2}$, $\rho = r/w_0$, the remaining symbols in Eqs. (1)–(6) have the following definitions:

$$E = E_0 e^{-r^2/w^2}; \quad w = w_0 \sqrt{1 + \zeta^2}, \quad (7)$$

$$C_n = \left(\frac{w_0}{w} \right)^n \cos(\psi + n\psi_G); \quad n = 1, 2, 3, \dots, \quad (8)$$

$$S_n = \left(\frac{w_0}{w} \right)^n \sin(\psi + n\psi_G), \quad (9)$$

where

$$\psi = \psi_0 + \omega t - kz - \frac{kr^2}{2R}; \quad R = z + \frac{z_r^2}{z}, \quad (10)$$

and ψ_0 is a *constant* initial phase. Also, t is the time and $k = 2\pi/\lambda$ is the wavenumber. On the other hand, with $E_0 \rightarrow E_{0l}$, the power expression may be given, to the same order in ε as the field components, by

$$P_l = \frac{\pi w_0^2 E_{0l}^2}{4 c \mu_0} \left[1 + \left(\frac{\varepsilon}{2} \right)^2 + 2 \left(\frac{\varepsilon}{2} \right)^4 + 6 \left(\frac{\varepsilon}{2} \right)^6 + \frac{45}{2} \left(\frac{\varepsilon}{2} \right)^8 + \frac{195}{2} \left(\frac{\varepsilon}{2} \right)^{10} \right], \quad (11)$$

where c is the speed of light in vacuum, μ_0 is the permeability of free space, and E_{0l} is the electric field amplitude, with l standing for *linearly polarized*. Note that $E_{0l} \propto \sqrt{P_l}$ and that the leading term in E_{0l} is inversely proportional to w_0 .

B. Radial polarization

Since focusing to a waist radius $w_0 < \lambda$ is key to achieving the high-energy gains we have in mind, it is only natural to seek modes of a Gaussian beam that may be focused to the tightest spot possible. It has recently been shown [17–19] that a (low-intensity) radially polarized beam may be focused down to a spot size $(0.16\lambda)^2$. This is better than the spot size of $(0.26\lambda)^2$ achieved for a linearly polarized beam. The spot size is defined as the area enclosed by a contour at which the beam intensity falls to one half its peak value.

The electric field of a radially polarized laser beam has two components, radial E_r and axial E_z , with propagation always along the z axis. In addition to that, only one magnetic field component, B_θ , which is azimuthal, exists. As will be demonstrated below, E_z works efficiently to accelerate the particles, while E_r and B_θ play a confining role and help to limit diffraction of the accelerated particle beam.

The reader will, likewise, be directed elsewhere [20] for the full expressions, in terms of the Gaussian beam parameters, of the fields of the radially polarized beam, otherwise referred to, sometimes, as an axicon beam. We quote here, too, only the leading terms of the field components:

$$E_r = E \{ \varepsilon \rho C_2 + \dots + O(\varepsilon^{11}) \}, \quad (12)$$

$$E_z = E \{ \varepsilon^2 [S_2 - \rho^2 S_3] + \dots + O(\varepsilon^{10}) \}, \quad (13)$$

$$B_\theta = \frac{E}{c} \{ \varepsilon \rho C_2 + \dots + O(\varepsilon^{11}) \}. \quad (14)$$

On the other hand, the power expression of the axicon beam, to order ε^{10} , takes on the following form

$$P_r = \frac{\pi w_0^2 E_{0r}^2}{2 c \mu_0} \left(\frac{\varepsilon}{2} \right)^2 \left[1 + 3 \left(\frac{\varepsilon}{2} \right)^2 + 9 \left(\frac{\varepsilon}{2} \right)^4 + 30 \left(\frac{\varepsilon}{2} \right)^6 + \frac{225}{2} \left(\frac{\varepsilon}{2} \right)^8 \right]. \quad (15)$$

Note here, too, that the radially polarized electric field amplitude $E_{0r} \propto \sqrt{P_r}$. Furthermore, when the definition of ε is used, one finds that the leading term in E_{0r} is independent of w_0 . The dependence upon w_0 of the field strength is shown in Fig. 1. Note that, whereas the linearly polarized field strength attains a maximum value beyond which it falls down with increasing waist radius, the radially polarized strength increases steadily to an asymptotic constant value.

III. SINGLE-PARTICLE TRAJECTORY CALCULATIONS

In this section the theory and background program of our calculations will be briefly outlined. Motion of a single particle of mass M and charge Q in the electric and magnetic fields \mathbf{E} and \mathbf{B} , respectively, of a laser beam will be considered classically, but relativistically. The use of laser systems of high intensity (in excess of 10^{18} W/cm²) leads to relativistic particle dynamics. Thus, the dynamics will be governed by the

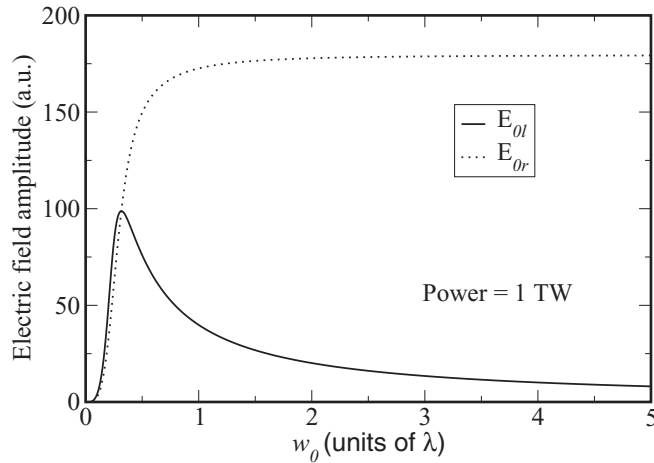


FIG. 1. Laser field strength at focus (E_{0l} for linear polarization and E_{0r} for radial polarization) as a function of the waist radius at focus.

Newton-Lorentz (or energy-momentum transfer) equations (SI units):

$$\frac{d\mathbf{p}}{dt} = Q[\mathbf{E} + c\boldsymbol{\beta} \times \mathbf{B}]; \quad \frac{d\mathcal{E}}{dt} = Qc\boldsymbol{\beta} \cdot \mathbf{E}, \quad (16)$$

in which the relativistic energy and momentum of the particle are given by $\mathcal{E} = \gamma Mc^2$ and $\mathbf{p} = \gamma M c \boldsymbol{\beta}$, respectively, with $\boldsymbol{\beta}$ its velocity scaled by c , and $\gamma = (1 - \beta^2)^{-1/2}$ its Lorentz factor. Out of many single-particle dynamical aspects, we are mainly interested in the energy gained by the particle as a result of interaction with a continuous laser beam. The case of pulsed lasers, which are able to produce the high powers needed, is treated in Sec. VII. To arrive at the energy gain, numerical solutions to the equations above will be sought. In most cases of practical utility, a solution proceeds along the following lines. First, the two equations are combined to give

$$\frac{d\boldsymbol{\beta}}{dt} = \frac{Q}{\gamma Mc} [(\mathbf{E} + c\boldsymbol{\beta} \times \mathbf{B}) - \boldsymbol{\beta}(\boldsymbol{\beta} \cdot \mathbf{E})]. \quad (17)$$

Then, in principle, a numerical integration of Eq. (17) yields $\boldsymbol{\beta}$ and, hence, γ_f at a later time t_f taken equal to many laser field cycles. Finally, one calculates the energy gain of the particle from

$$G = (\gamma_f - \gamma_i)Mc^2, \quad (18)$$

where $\mathcal{E}_i = \gamma_i Mc^2$ is the initial (injection) energy.

Energy carried by an optical photon of wavelength $\lambda \sim 1 \mu\text{m}$ is of the order of 1 eV, much smaller than a typical nuclear excitation energy. So, barring multiphoton absorption, these charge states remain *intact* in, and get accelerated by, the strong electromagnetic fields of present-day laser intensities already in excess of 10^{22} W/cm^2 . It should be noted that, with the applications in mind, we treat the acceleration of bare nuclei; the behavior of ions which are not fully stripped may be more complex due to strong-field ionization processes.

The procedure outlined above has been used extensively to study acceleration of electrons by linearly polarized laser fields [21]. The same procedure has been followed recently in investigating possible acceleration of electrons by radially polarized laser fields [20]. In the latter calculations, however,

single-particle dynamics only were emphasized and a set of artificial initial conditions (rest at the origin of coordinates) was used in most cases. From the single-particle calculations, one learned that electron laser acceleration to GeV energy is possible. As it has been explained [21,22], the use of focused fields circumvents the Lawson-Woodward theorem [23], which predicts zero net acceleration in the case of an infinite plane wave. Study of individual particle trajectories showed that most of the energy gain takes place during interaction with a small number of laser field cycles. In addition to that, the role of laser focusing has been thoroughly discussed. Dependence of the gain on the initial phase ψ_0 of the fields was also demonstrated. Maximum gain from high-intensity laser fields required that the particles be injected into the focal region at space-time points corresponding to the neighborhood of some specific value of ψ_0 , allowing the particles to *surf* on the laser waves and gain energy from them. Failing to meet the conditions of the right value of ψ_0 results in *phase slippage* and can even lead to negative deceleration. An optimum ψ_0 value has to be determined for each set of initial conditions, particle charge, laser polarization, and laser power. For example, for particles *released from rest* near the beam focus (and origin of coordinates), maximum gain may be obtained from radially polarized fields for $\psi_0 \approx \pi$, for negatively charged entities, and $\psi_0 \approx 0$ for positively charged ones. These values correspond to space-time points at which the particle is initially subjected to the accelerating field minimum.

This paper is about laser acceleration of bare nuclei [12,20]. We wish to develop the study of direct laser acceleration of bare nuclei by introducing fluctuations in the initial positions and momenta of the particles [12] and employing the most accurately represented fields [16,20].

An approximate value for the magnitude of energy gain that may be achieved using present-day laser systems can be obtained from estimate formulas. Consider a nucleus of charge $+Ze$, where Z is the atomic number, near the focus of a linearly polarized laser beam, itself the origin of coordinates. According to Eqs. (1)–(6) the fields are transverse near the focus, with E_x and B_y being the only nonvanishing components. So, together with the magnetic force, the force due to E_x will act to accelerate the nucleus. An approximate expression for the energy gain may then be obtained from the second of Eqs. (16), which now reads $d\mathcal{E}/dt \approx Qc\beta_x E_x$. Taking $\beta_x \sim 1$, an exaggeration that will result in the final expression overestimating the gain, and recognizing that in this limit, $E \sim E_0$ and $S_1 \sim \sin(\omega t)$, the approximate equation may now be formally integrated with respect to time. The final result will then yield the following approximate expression for the maximum gain per nucleon, in MeV, when the laser power is given in terawatt (TW)

$$G_l[\text{MeV/nucleon}] \sim \frac{2Z}{A} \left(\frac{\lambda}{\pi w_0} \right) \sqrt{30P_l[\text{TW}]}, \quad (19)$$

where A is the atomic number and the field strength E_{0l} has been replaced by its value from the leading term in the power Eq. (11). As an example, a nucleus of $^{12}_6\text{C}$, or any nucleus having the same charge-to-mass ratio $Z/A = 0.5$, will gain approximately 3.63 MeV/nucleon from a 1-TW laser focused to a waist radius $w_0 = 0.48\lambda$. A proton, on the other hand,

would gain about 7.26 MeV from the same laser. As will be demonstrated below, these numbers are at least one order of magnitude greater than the results of calculations that employ the accurate fields. In addition to employing the values of the fields right at the focus, this must also be due, in part, to setting $\beta_x \sim 1$ in arriving at Eq. (19).

Similar analysis involving the radially polarized fields Eqs. (12)–(14) gives the following approximate expression for the maximum gain:

$$G_r [\text{MeV/nucleon}] \sim \frac{Z}{A} \left(\frac{\lambda}{\pi w_0} \right)^2 \sqrt{240 P_r [\text{TW}]} \quad (20)$$

According to this expression, a carbon nucleus in a 1-TW field focused to $w_0 = 0.48\lambda$ achieves a gain $G_r \sim 3.41$ MeV/nucleon, which is slightly smaller than what would be obtained from a linearly polarized field of the same parameters. On the other hand, the gain by a proton would be $G_r \sim 6.81$ MeV. In fact, a comparison of Eqs. (19) and (20) shows that G_r will be greater than G_l as long as $w_0/\lambda < \sqrt{2}/\pi \sim 0.45$. Unfortunately, only low-intensity radially polarized beams may be generated in the laboratory at present [17–19].

IV. THE SIMULATIONS

In this section the full power of the accurate field expressions will be used to study the dynamics of bare nuclei on the basis of Eq. (16). A simple estimate [24] reveals that the interparticle Coulomb force, F_C , between a pair of, say, protons in an ensemble of the sort described above is small compared to the force, F_L , felt by a particle of the same type from the laser electric field. For the laser-field intensities used in our calculations in this paper, $F_C \ll F_L$ for any ionic charge state. Furthermore, as it has been shown by simulations including the interionic interaction in the relativistic equations of motion [25], at the low particle densities considered in our simulations ($\sim 10^{17}$ ions/cm³), even the field-free evolution of the ionic ensemble after acceleration is only negligibly influenced by ion-ion interaction effects.

We consider an ensemble of N *noninteracting* particles initially in a cylinder of radius R_c and length L_c oriented along the laser beam axis, taken as the z axis, and centered on the origin of coordinates as shown in Fig. 2. The initial position coordinates (x_0, y_0, z_0) will be taken as uniformly distributed within the cylinder (but will be picked at random in our numerical simulations). The particles will be assumed to possess initial kinetic energies distributed normally around a mean value \bar{K} and having a spread ΔK . Without any loss of generality, the initial motion of all particles will be taken in the xz plane and at some angle θ_i with respect to the beam axis.

Our interest, in this paper, is mainly in the energy gain, or exit kinetic energy, of the nuclei, their trajectories, and, hence, the aspects that determine the quality of an accelerated beam of such accelerated nuclei. In the next two sections we study the laser acceleration of four nuclear species, namely hydrogen, helium, carbon, and oxygen in some detail.

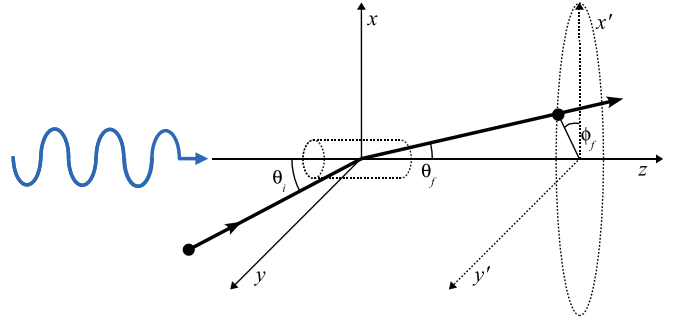


FIG. 2. (Color online) A schematic diagram showing the geometry of laser acceleration of nuclei. θ_i and θ_f represent the injection and the ejection angle of the particles, respectively.

V. ACCELERATION BY A LINEARLY POLARIZED LASER BEAM

Intense high-energy proton beams are widely generated by irradiating solid surfaces with intense laser light [7,26–34]. The mechanism at work in these experiments is the target normal sheath acceleration (TNSA). Very hot electrons are generated and are driven into the bulk of the target by the laser pulse. Once they leave the rear surface of the target, the charge separation between the electrons and the positive ions they leave behind generates a strong quasistatic electric field, leading to efficient ion (proton) acceleration. In our work, alternatively, the method is one of acceleration in vacuum by subjecting the particles directly to the laser beam. In all our simulations, the wavelength will be taken as $\lambda = 10.6 \mu\text{m}$, corresponding to a CO₂ laser. Choosing a wavelength larger than the conventional range around $1 \mu\text{m}$, which characterizes titanium-sapphire and Nd:YAG lasers, is motivated by the fact that the focal volume increases approximately as $\propto \lambda^3$, which allows for three orders of magnitude more particles to be accelerated by the laser pulse as one bunch. Note that, for $w_0 \sim \lambda$, the Rayleigh length $z_r = \pi w_0^2/\lambda \sim \pi\lambda$. In our calculations, however, focusing will be to a waist radius $w_0 = 0.48\lambda$. Note that the peak intensity of a linearly polarized 100-TW laser system, focused to this level, is already $I \sim 2.14 \times 10^{20}$ W/cm². We consider an initial ensemble of $N = 5000$ particles injected at an angle $\theta_i = 10^\circ$ relative to the beam axis. The particles have a mean kinetic energy $\bar{K} = 10$ keV and a spread $\Delta K = 10$ eV. The initial coordinates of the particles will be randomly picked from within a cylinder of length $L_c = 1 \mu\text{m}$ and radius $R_c = 0.1 \mu\text{m}$ [12].

Results from single-particle calculations are presented in Fig. 3. The particle in each case is selected at random from the ensemble described above. In this figure, the kinetic energy, $K \equiv Mc^2(\gamma - 1)$, of each particle is shown as it evolves along the x axis of its trajectory. Note that the exit kinetic energy, at the end of the particle trajectory, displayed in Fig. 3 is about ten times greater than the estimates made above. Such a deviation is not surprising, given that in the simulations we considered tightly focused fields rather than plane waves. As the laser power is tuned from 0.1 to 10 PW, a proton's exit kinetic energy increases roughly from 4 to 523 MeV. On the other hand, evolution of the kinetic energies of all the other nuclear species, as well as their exit values, are more or less the same. This should come as no surprise because the gain

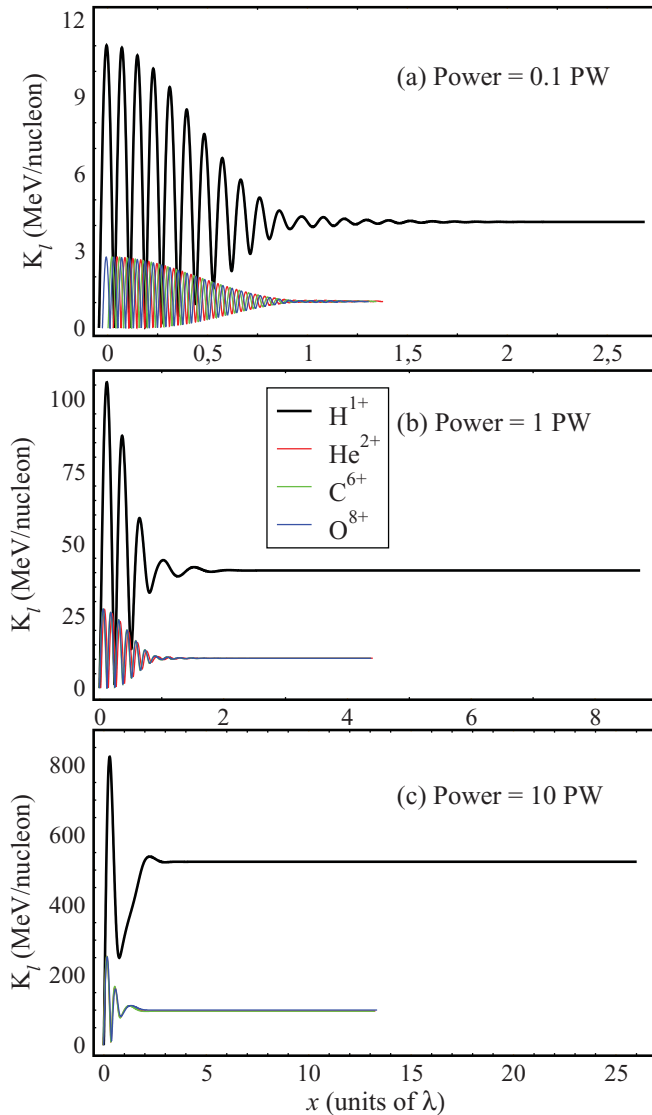


FIG. 3. (Color online) Evolution of the kinetic energies of four nuclear species in linearly polarized laser fields as functions of their excursion distances along the laser polarization direction. The laser wavelength is $\lambda = 10.6 \mu\text{m}$ and the beam waist radius at focus is $w_0 = 0.48\lambda$. The given powers (0.1, 1, and 10 PW) correspond to peak intensities $I \sim 2.14 \times 10^{20}$, 2.14×10^{21} , and $2.14 \times 10^{22} \text{ W/cm}^2$, respectively. Injection angle is $\theta_i = 10^\circ$ for all particles. Integration of the equations of motion was carried out over a range of values $\Delta\eta = 60\pi$ of the variable $\eta \equiv \omega(t - z/c)$.

depends on the charge-to-mass ratio Z/A , as shown in the qualitative analysis [Eqs. (19) and (20)]. This ratio is exactly 0.5 for helium (He), carbon (C), and oxygen (O), while it is equal to unity in the case of the proton. The exit kinetic energies of the He, C, and O nuclei increase from roughly 1 to 97 MeV/nucleon as the laser power is increased from 0.1 to 10 PW. Note that while laser powers in the 0.1- to 1-PW regime are readily available today, powers of the order of tens of PWs will be provided by upcoming facilities [35,36]. Also, the problem of focusing to subwavelength waist radii at such powers is yet to be resolved.

In Fig. 4(a), evolution of the kinetic energy of a nucleus of oxygen (O^{8+}) is shown as a function of the time. Note

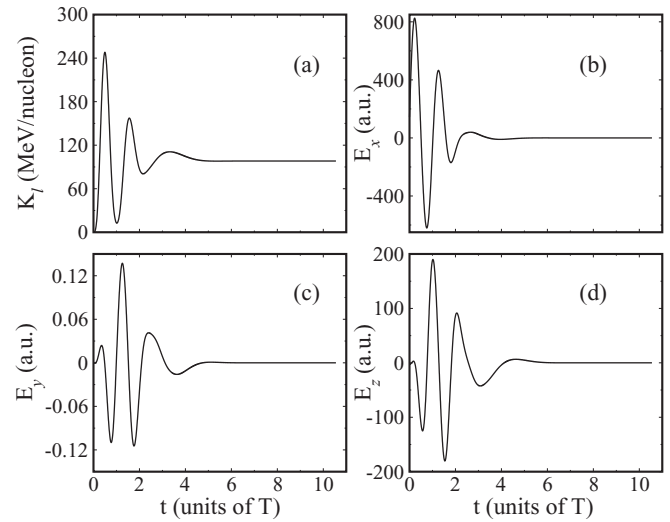


FIG. 4. (a) Kinetic energy of a nucleus of oxygen as a result of interaction with a linearly polarized 10 PW laser beam, and (b)–(d) the electric field components E_x , E_y , and E_z , respectively, seen by the particle along its trajectory as functions of the time in units of T , the laser period. Integration of the equations of motion was carried out over a range of values $\Delta\eta = 20\pi$ of the variable $\eta \equiv \omega(t - z/c)$. The remaining parameters are the same as described in the legend of Fig. 3.

that interaction of the particle with the 10-PW laser field is substantial only over a few laser field cycles. No appreciable energy is gained beyond that. To see which laser electric field components were most effective in the acceleration process, we plot the strengths of all three components along the particle trajectory in Figs. 4(b)–4(d). During the interaction, the figures show that, for the parameter set employed, E_x has been most effective in accelerating the particle, E_y more than 3 orders of magnitude less effective, while E_z has mostly played a negative (decelerating) effect.

For the purpose of illustration, we show trajectories of 100 particles from the ensemble, in Fig. 5. The particles are accelerated in the direction of the resultant \mathbf{E} field, from which they gain the most energy. With time, a particle develops substantial momentum and the $\mathbf{v} \times \mathbf{B}$ begins to affect its direction of motion. Thus, wiggles in the trajectories show up over the part of the figure that corresponds to effective interaction, which is a few field cycles at most, followed by particle motion along essentially straight lines. The effect of all the force components causes the trajectories to lie within a wedge-like structure of an approximately rectangular cross section.

Shown in Fig. 6 are kinetic energies of the particles whose trajectories are displayed in Fig. 5. Note that the spread in the exit kinetic energies is quite small. More on this topic will be found below.

Next, effect of the acceleration process on an ensemble of 5000 alpha particles will be discussed. In Fig. 7, we show the positions to which the ensemble evolves as a result of the acceleration mechanism, together with the exit kinetic energies of its members. For example, Figs. 7(a)–7(c) give the coordinates (z_f, y_f) at the ends of the 5000 trajectories. As the laser power increases, the (roughly) rectangular end beam cross-section grows in size, indicating an increase in particle beam divergence. The cross-section also shifts center

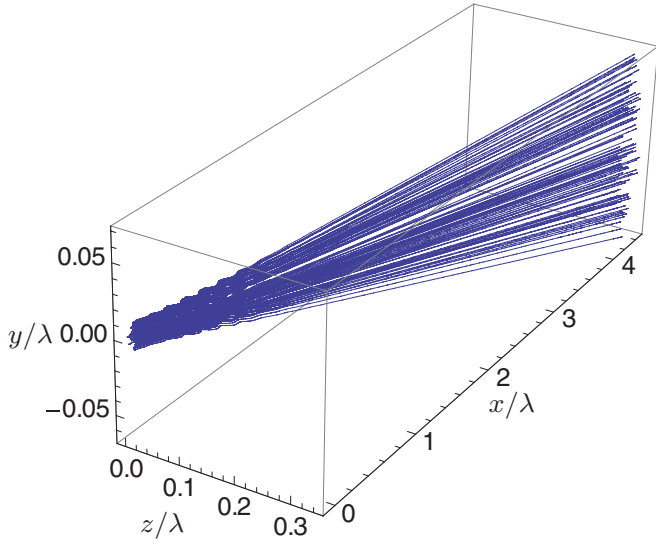


FIG. 5. (Color online) 3D trajectories of 100 He²⁺ nuclei (alpha particles) in a 1-PW linearly polarized laser beam. All other parameters are the same as described in the legend of Fig. 3.

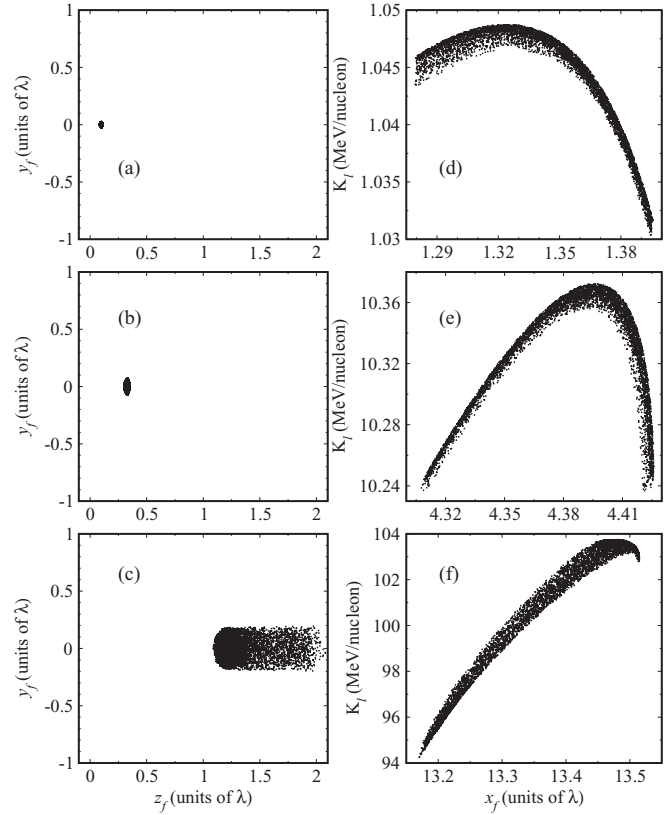


FIG. 7. (a)–(c) Accelerated particle beam cross-sections in the yz plane, and (d)–(f) exit kinetic energies of the accelerated particles vs. the total excursion distance along the laser polarization direction. The laser power used in producing each row of figures is 0.1, 1, and 10 PW (top to bottom). The initial ensemble consists of 5000 He²⁺ nuclei (alpha particles) in a cylinder of length $L_c = 1 \mu\text{m}$ and radius $R_c = 0.1 \mu\text{m}$. All other parameters are the same as described in the legend of Fig. 3.

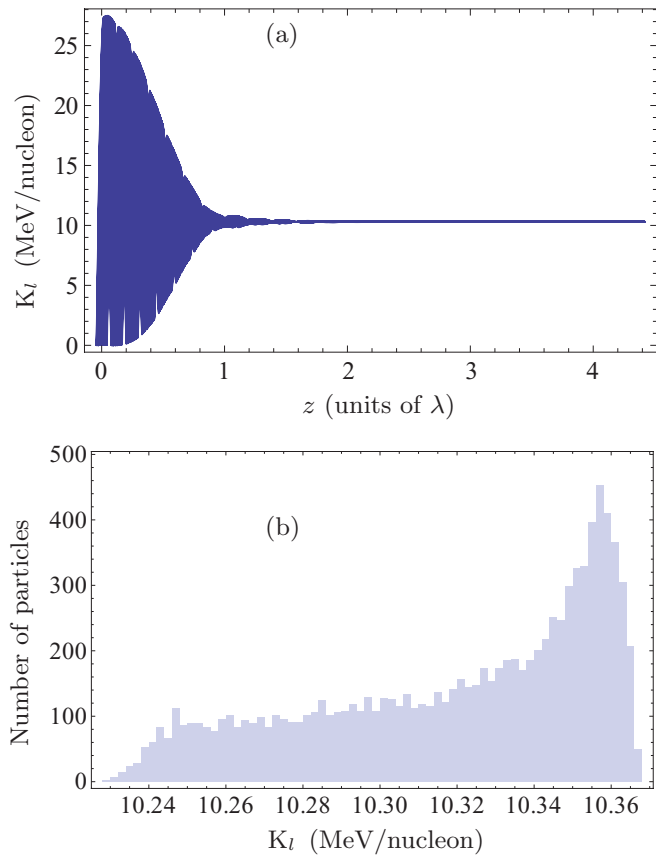


FIG. 6. (Color online) (a) Exit kinetic energies of 100 He²⁺ nuclei (alpha particles) in a 1-PW linearly polarized laser beam vs. the excursion of each along the x axis (the laser polarization direction). (b) The distribution of final kinetic energies of 10 000 alpha particles (equivalent to two bunches of 5000 particles each). All other parameters are the same as described in the legend of Fig. 3.

(to the right), which indicates the overall combined effect of the laser E_z and magnetic field components. This is also accompanied by the expected increase in the energy gain and final x excursion. Figures 7(d)–7(f) give the exit kinetic energies (at ends of trajectories) against the exit coordinate x_f . Note here, too, that the spread in exit kinetic energies is quite small, so is the spread in the excursion distance along the polarization direction. These points will be discussed further below, in connection with the suitability of a particle beam for use in radiotherapy.

For the purpose of further discussion of the results, we denote by $\bar{x}_f, \bar{y}_f, \bar{z}_f$, and \bar{K}_f , the ensemble averages of the exit coordinates x_f, y_f, z_f and exit kinetic energy K_f , respectively, at the end of the trajectories. Furthermore, $\Delta x_f, \Delta y_f, \Delta z_f$, and ΔK_f will denote the standard deviations in these quantities. As usual, a standard deviation will represent a measure of the spread in the quantity in question. According to Figs. 7(a)–7(c), the final position coordinates in the zy plane are randomly distributed in a region of space that may be approximated by rectangles whose sides can be estimated by $2\Delta z_f$ and $2\Delta y_f$. Recognizing that \bar{x}_f is the largest excursion made by a particle along one of the three coordinate axes, we may also speak of a solid angle, defined approximately for our purposes here

TABLE I. Particle coordinates, beam solid angles, and kinetic energies at the ends of the trajectories of helium nuclei accelerated by linearly polarized laser beams. Results shown here are derived from the data used to produce Fig. 7.

Power (PW)	\bar{x}_f (units of λ)	\bar{y}_f (units of λ)	\bar{z}_f (units of λ)	$\Delta\Omega$ (sr)	\bar{K}_f (MeV/nucleon)
0.1	1.34 ± 0.03	0.00 ± 0.01	0.10 ± 0.01	1.9×10^{-4}	1.044 ± 0.005
1	4.38 ± 0.03	0.00 ± 0.03	0.33 ± 0.01	8.1×10^{-5}	10.33 ± 0.04
10	13.37 ± 0.10	0.00 ± 0.09	1.39 ± 0.22	4.7×10^{-4}	100.8 ± 2.8

by $\Delta\Omega \simeq (2\Delta z_f)(2\Delta y_f)/\bar{x}_f^2$. Final mean position coordinates and the spread in each, in units of the laser wavelength λ , the approximate solid angle, in sr, and the kinetic energy and spread in it, in MeV/nucleon, are collected in Table I, for the

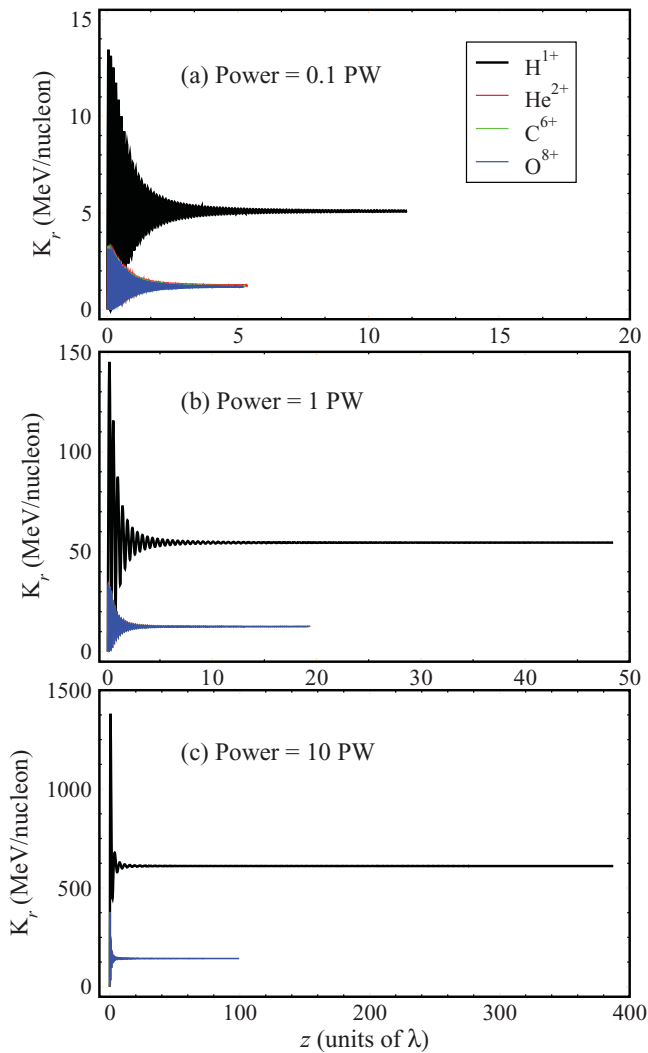


FIG. 8. (Color online) Evolution of the kinetic energies of four nuclear species in radially polarized laser fields as functions of their excursion distances along the laser propagation direction. The laser wavelength is $\lambda = 10.6 \mu\text{m}$ and the beam waist radius at focus is $w_0 = 0.48\lambda$. The given powers (0.1, 1, and 10 PW) correspond to peak intensities $I \sim 7.41 \times 10^{19}$, 7.41×10^{20} , and $7.41 \times 10^{21} \text{ W/cm}^2$, respectively. (Strictly, at points on the transverse plane through the focus where $z = 0$ and $r \sim w_0/\sqrt{2}$). Injection angle is $\theta_i = 10^\circ$ for all particles. Integration of the equations of motion was carried out over a range of values $\Delta\eta = 200\pi$ of the variable $\eta \equiv \omega(t - z/c)$.

data of Fig. 7. Note that the spread in exit kinetic energy is ~ 0.5 , 0.4 , and 2.8% , respectively, in the three cases considered.

In comparison to these results, according the combined experimental-theoretical study of Ref. [37], TNSA produces similar maximal proton kinetic energies. At the laser intensities given in Fig. 8, TNSA results in kinetic energies of around 20, 60, and 250 MeV (see Fig. 1(a) of Ref. [37], showing results for a laser of a wavelength $1.054 \mu\text{m}$), with energy spreads of the order of 20–30%, which is to be compared to our results of 5.1, 55, and 590 MeV, respectively (see Fig. 8). Thus, while our direct ion acceleration scheme is outperformed by TNSA at lower intensities, it leads to higher kinetic energy gains at the highest intensity of $7.41 \times 10^{21} \text{ W/cm}^2$, and generally to much lower energy spreads (see Table I). More efficient acceleration has been predicted by RPA schemes; e.g., in Ref. [38], a relativistic acceleration regime is suggested which leads to GeV/nucleon ion energies at an intensity of 10^{22} W/cm^2 .

VI. ACCELERATION BY A RADIALLY POLARIZED LASER BEAM

Two characteristics give the radially polarized beam an edge over the linearly polarized one. It can be focused to a tighter spot, and it has three field components: one mainly responsible for the acceleration and the other two working to *confine* the particles and limit the transverse particle-beam diffraction. The tighter spot means a higher peak intensity (see Fig. 1) and, hence, leads to better gain. On the other hand, the axial electric field component, E_z , which is mainly responsible for the acceleration, increases in strength with tighter focusing at the expense of the radial component E_r and the azimuthal magnetic component B_θ . Recall that both E_r and B_θ vanish identically on the beam axis, leaving E_z to work effectively alone to accelerate the particles.

Consequently, due to its geometrical properties, a radially polarized laser beam is somewhat better suited for the purpose of acceleration than a linearly polarized beam. Unfortunately, generation of high-intensity radially polarized light is still a challenge [17–19]. Nevertheless, assuming such beams can be produced in the near future, we will present and discuss below results of numerical simulations similar to the ones considered above, albeit for radially polarized beams.

To begin with, Fig. 8, in which evolution of the particle kinetic energies along the laser beam direction of propagation, is similar to Fig. 3. Note first that, by comparison, the exit kinetic energies in this case are slightly higher than in the linearly polarized case. The end particle coordinates (along the laser beam axis) are also greater than the excursion distances along the linearly polarized beam polarization direction. This

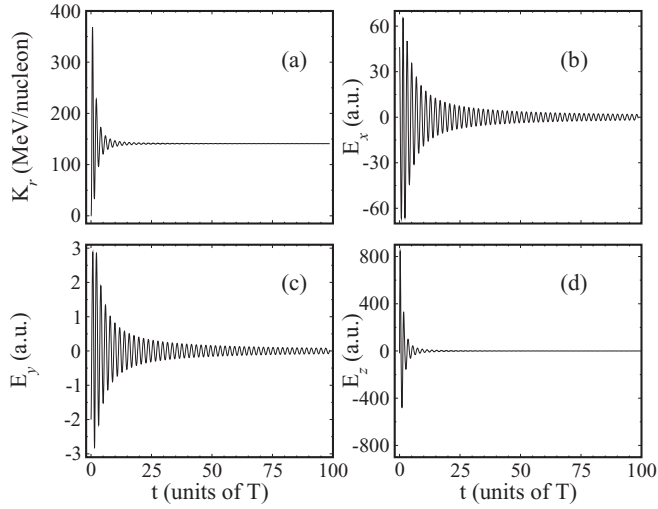


FIG. 9. Same as described in the legend of Fig. 4, but for a radially polarized beam. Note that $E_x = E_r \cos \theta$ and $E_y = E_r \sin \theta$, where $\theta = \arctan(y/x)$. Integration of the equations of motion was carried out over a range of values $\Delta\eta = 100\pi$ of the variable $\eta \equiv \omega(t - z/c)$. The remaining parameters are the same as described in the legend of Fig. 8.

hints at the strength of the axial electric field component, E_z , and its role in the acceleration process.

Further insight into the nature of the trajectories may be gained from Fig. 9 that will shed light on the accelerated particle beam quality. The first thing to note is the increase in transverse spreading, in the xy plane, with increasing laser power. This divergence may also be assessed in terms of a solid angle defined roughly by $\Delta\Omega \simeq (2\Delta x_f)(2\Delta y_f)/z_f^2$, where the area covered by the points is considered as a rectangle of sides $2\Delta x_f$ and $2\Delta y_f$. Figure 9 is to be compared with Fig. 4. Note

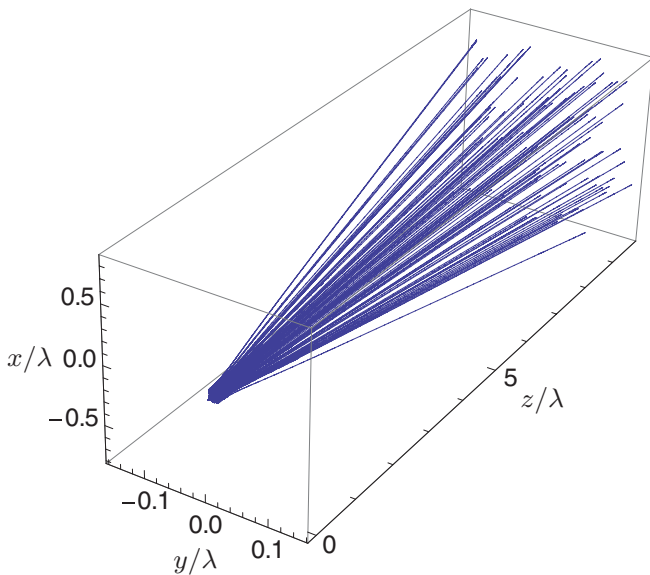


FIG. 10. (Color online) Same as described in the legend of Fig. 5, but for a radially polarized laser system and the excursion distance is along the z axis. Integration of the equations of motion was carried out over a range of values $\Delta\eta = 100\pi$ of the variable $\eta \equiv \omega(t - z/c)$.

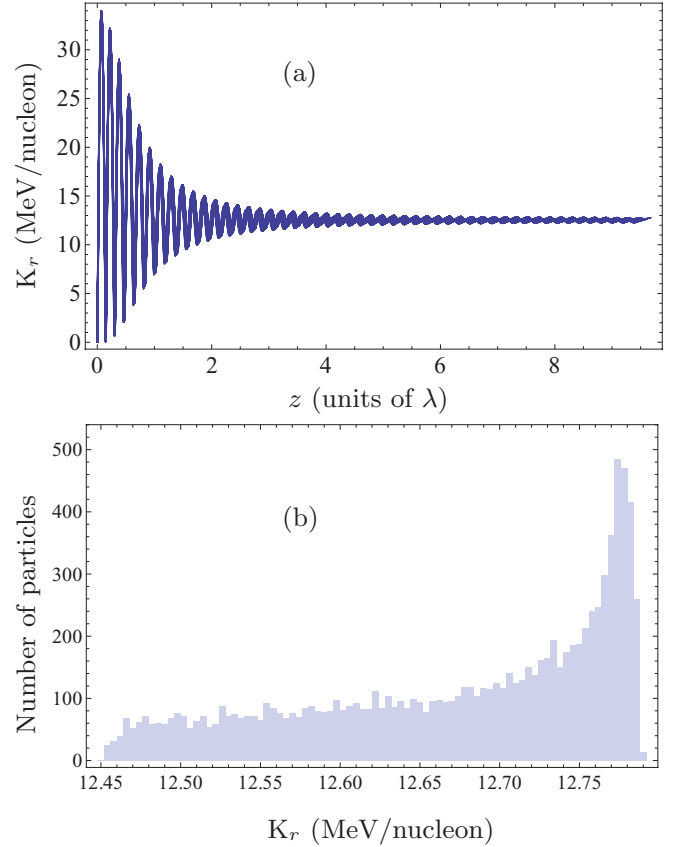


FIG. 11. (Color online) Same as described in the legend of Fig. 6, but for a radially polarized laser system and the excursion distance is along the z axis. Integration of the equations of motion was carried out over a range of values $\Delta\eta = 100\pi$ of the variable $\eta \equiv \omega(t - z/c)$.

that E_z is the strongest component and from reading Fig 9(a) and 9(d) together, one concludes that E_z is the accelerating field component, while E_r (or equivalently its components, in this context, E_x and E_y) plays a minor role.

Figures 10 and 11 are similar to Figs. 5 and 6. The rectangular shape taken by the beam cross section in Fig. 10 seems to be sharper than in Fig. 5. This conclusion is also supported by Fig. 12, which is the analog of Fig. 7. Evolution of the kinetic energy with excursion distance, as shown in Fig. 11, seems to suggest that the spread in exit energies is smaller in the radially polarized case than it is in the corresponding linearly polarized counterpart. Support for this conclusion may be found by comparing Figs. 12(d)–12(f) with 7(d)–7(f).

Results from our simulations employing radially polarized beams, paralleling those displayed in Table I for the linearly polarized case, are shown in Table II. One observes an increase in energy gain with increasing power, as expected. Note that the spread in the exit kinetic energies is less than 1% in all of the three cases considered. Comparing corresponding items in Tables I and II, one finds that the radially polarized fields result in more energy gain compared to the linearly polarized ones.

VII. INITIAL ION DISTRIBUTION AND PULSE-SHAPE EFFECTS

We performed simulations to study the effect of different volumes of the initial ion distribution on the energy spread

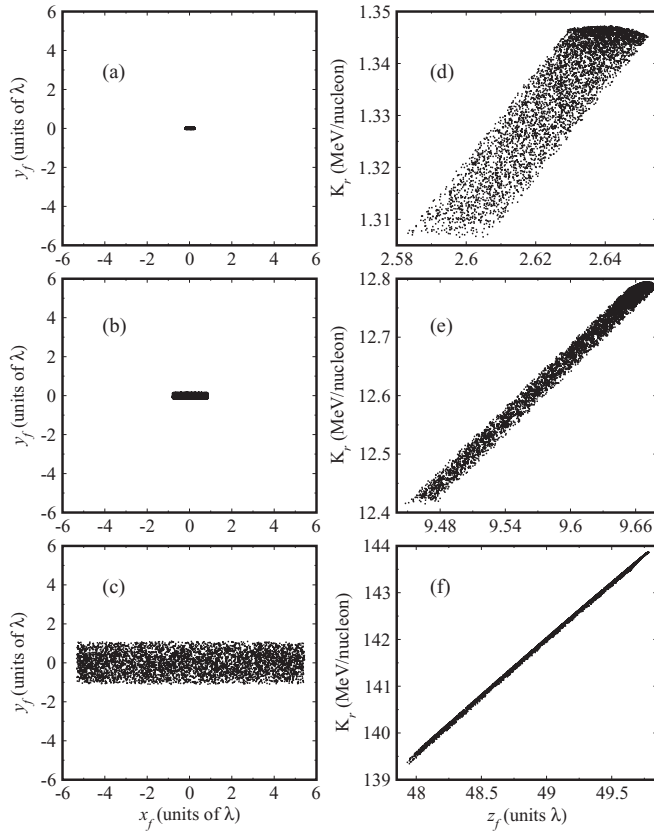


FIG. 12. Same as described in the legend of Fig. 7 but for acceleration employing a radially polarized beam.

of the accelerated particles. The size (volume) of the initial cylinder ($L_c = 1 \mu\text{m}$, $R_c = 0.1 \mu\text{m}$) has been increased by factors of 2, 4, and 8, while keeping the other parameters fixed. Table III shows the result of these calculations for a laser power of 10 PW. Given are the average final kinetic energies together with their spreads (standard deviations) and the percentage energy spread. As can be seen, the increase of the initial volume has a twofold effect: the average energy is slightly lowered and its spread increases significantly, roughly linearly. The values in the table give the tolerances on the size of the initial ionic distribution. As can be seen in Table III, ions accelerated by radially polarized fields are somewhat more tolerant to the increase in size of the interaction region, thus allowing for the acceleration of a larger number of particles, while keeping kinetic energy and energy spread under control.

In addition, we performed simulations which employ laser systems that provide their energy in pulses of finite duration

TABLE II. Particle coordinates, beam solid angles, and kinetic energies at the ends of the trajectories of helium nuclei accelerated by radially polarized laser beams. Results shown here are derived from the data used to produce Fig. 12.

Power (PW)	\bar{x}_f (units of λ)	\bar{y}_f (units of λ)	\bar{z}_f (units of λ)	$\Delta\Omega$ (sr)	\bar{K}_r (MeV/nucleon)
0.1	0.03 ± 0.12	0.00 ± 0.02	2.63 ± 0.01	1.6×10^{-3}	1.334 ± 0.011
1	0.02 ± 0.48	0.00 ± 0.09	9.60 ± 0.06	1.8×10^{-3}	12.67 ± 0.11
10	0.01 ± 3.13	0.00 ± 0.55	49.15 ± 0.52	2.9×10^{-3}	142.3 ± 1.2

TABLE III. Dependence of the average final kinetic energy \bar{K} and the relative kinetic energy spread $\Delta K/\bar{K}$ on the volume of the initial distribution. The size of the initial ionic distribution is given as a multiple of the volume defined in the text. The protons and alpha particles are interacting with linearly (l) or radially (r) polarized light.

	Size	\bar{K}_l (MeV/nucleon)	$\Delta K_l/\bar{K}_l$ (%)	\bar{K}_r (MeV/nucleon)	$\Delta K_r/\bar{K}_r$ (%)
H^{1+}	$1 \times$	416.7 ± 24.4	5.9	532.8 ± 13.3	2.5
	$2 \times$	416.2 ± 50.6	12	530.1 ± 16.8	3.2
	$4 \times$	403.3 ± 86.9	22	527.2 ± 20.9	4.0
	$8 \times$	359.2 ± 152	42	517.6 ± 29.0	5.6
He^{2+}	$1 \times$	90.65 ± 0.93	1.0	122.0 ± 1.0	0.8
	$2 \times$	90.49 ± 1.70	1.9	121.4 ± 1.5	1.2
	$4 \times$	90.20 ± 2.73	3.1	120.2 ± 2.4	2.0
	$8 \times$	89.78 ± 4.51	5.0	118.8 ± 3.7	3.1

and compared the results with those obtained using continuous wave (cw) lasers, keeping all other parameters fixed. To lowest order in the time, a pulse shape can be introduced by multiplying the laser fields with the phase-dependent factor $g(\eta)$, where $\eta = \omega t - kz$, effectively via the following transformations:

$$\begin{aligned} \mathbf{E} &\rightarrow g(\eta)\mathbf{E}, \\ \mathbf{B} &\rightarrow g(\eta)\mathbf{B}. \end{aligned} \quad (21)$$

Following K. T. McDonald [39], the following pulse-shape factor has been chosen:

$$g(\eta) = \text{sech}\left(\frac{\eta}{\eta_0}\right). \quad (22)$$

This choice justifies using the ansatz given by Eq. (21) in the limit $\eta_0 \gg 1$ [39]. The dimensionless phase parameter η_0 can be directly related to the pulse duration τ , itself taken as the full width at half maximum (FWHM), via the relation

$$\eta_0 = \omega\tau / \ln\left[\frac{2 + \sqrt{3}}{2 - \sqrt{3}}\right], \quad (23)$$

with ω the laser frequency. In order to fulfill the condition $\eta_0 \gg 1$, we chose a pulse duration $\tau = 0.25$ ps (approximately equivalent to 7 laser cycles for $\lambda = 10.6 \mu\text{m}$). For this choice, $\eta_0 \approx 16.9 \gg 1$. Infrared laser pulses with a pulse duration on the ps scale and with TW powers can be generated experimentally (see, e.g., Ref. [14]), and an extension to higher powers is anticipated in the near future.

Table IV summarizes the results of our simulations on the pulse-shape effects. Listed are the average final kinetic energies together with their spreads for carbon and oxygen

TABLE IV. Average and standard deviation of the final kinetic energies of carbon and oxygen bare nuclei accelerated by linearly and radially polarized laser fields. Acceleration cases corresponding to cw and pulsed fields are compared, using 5-PW laser systems focused to waist radii $w_0 = \lambda/2$.

	\bar{K}_l (MeV/nucleon)		\bar{K}_r (MeV/nucleon)	
	cw	Pulsed	cw	Pulsed
	$\tau = 0.25$ ps			
C ⁶⁺	46.36 ± 0.15	42.58 ± 0.42	57.54 ± 0.50	57.55 ± 0.50
O ⁸⁺	46.35 ± 0.15	42.56 ± 0.43	57.50 ± 0.50	57.50 ± 0.50
	$\tau = 0.5$ ps			
C ⁶⁺	46.36 ± 0.15	45.13 ± 0.22	57.54 ± 0.50	57.54 ± 0.50
O ⁸⁺	46.35 ± 0.15	45.12 ± 0.22	57.50 ± 0.50	57.50 ± 0.50

nuclei. It can be seen that the introduction of a pulse-shape has negligible influence in the case of the longer pulse $\tau = 0.5$ ps (for both polarizations). Whereas in the case of the shorter pulse $\tau = 0.25$ ps, only the results for the radially polarized laser fields remain effectively unchanged. For the pulsed linearly polarized case, the energy is roughly 8% lower than when the cw systems are used, and the energy spread is more than doubled but still remaining less than 1% in any case.

VIII. CONCLUSIONS

In this paper, theoretical calculations for electron laser acceleration, started earlier [20,21], have been extended to cover similar configurations involving bare nuclei, by numerically solving the relativistic equations of motion of the particles in radially and linearly polarized laser fields. The main results include acceleration of bare nuclei of hydrogen, helium, carbon, and oxygen to energies ranging from a few to several hundred MeV/nucleon, using laser systems of power 0.1–5 PW, focused down to waist radii in the neighborhood of half a laser wavelength ($w_0 \sim \lambda/2$). For the charge species studied, the radially polarized fields have been shown to lead to slightly higher energy gains than would be obtained using the linearly polarized fields. The linearly polarized fields, however,

lead to a lower spread in the particle beam energy gain, at least for the parameter sets employed in our simulations.

Recognizing that a radially polarized beam may be focused to a tighter spot than would be the case for a linearly polarized one, our results suggest that a laser beam of radial polarization may be a better candidate for use in laser acceleration of ions and bare nuclei, for medical and other applications. It has also been demonstrated that focusing even a 100-TW laser beam to a subwavelength spot radius increases its peak intensity to the levels needed for acceleration of bare nuclei.

Furthermore, choosing a laser system with a wavelength as long as possible is shown to increase the interaction volume of the focused light beam and the initial ionic ensemble, which leads to a higher number of particles accelerated in one bunch at a given initial ionic density. As an example, CO₂ lasers with a wavelength of 10.6 μm accelerate three orders of magnitude more particles in one shot as the most wide-spread systems with wavelengths around 1 μm , making these systems more appealing for ion acceleration applications once the power of these laser systems reaches the range required.

Finally, calculations have been performed in order to assess the effect, on the kinetic energies of the accelerated particles, due to variations in volume of the initial ionic distribution, and to an added pulse-shape on the laser systems employed. Our investigations prove that for sufficiently long pulses with a duration over 0.25 ps, the pulse shape effects are negligibly small, especially in the case employing laser fields of the radially polarized variety.

ACKNOWLEDGMENTS

The work of Z.H. was supported by the Helmholtz Alliance Program of the Helmholtz Association, Contract No. HA216/EMMI, “Extremes of Density and Temperature: Cosmic Matter in the Laboratory.” Y.I.S. acknowledges with thanks support for this project from the German Alexander von Humboldt Stiftung and from the Arab Fund for Economic and Social Development (State of Kuwait) through a Distinguished Scholar Award.

- [1] S. Fritzler, K. Ta Phuoc, V. Malka, A. Rousse, and E. Lefebvre, *Appl. Phys. Lett.* **83**, 3039 (2003).
- [2] X. Y. Peng *et al.* *Phys. Rev. E* **74**, 036405 (2006).
- [3] O. Jäkel, D. Schulz-Ertner, C. P. Karger, P. Heeg, and J. Debus, *Nucl. Instrum. Methods Phys. Res., Sect. B* **241**, 717 (2005); S. E. Combs *et al.*, *Cancer* **115**, 1348 (2009); O. Jäkel, M. Krämer, C. P. Karger, and J. Debus, *Phys. Med. Biol.* **46**, 1101 (2001); [http://www.gsi.de/portrait/beschleunigeranlage_e.html]; [<http://www.wanjiehospital.com/proton/program.htm>].
- [4] A. Alves, P. Reichart, R. Siegle, P. N. Johnston, and D. N. Jamieson, *Nucl. Instrum. Methods Phys. Res., B* **249**, 730 (2006).
- [5] K. W. D. Ledingham, P. McKenna, and R. P. Singhal, *Science* **300**, 1107 (2003).
- [6] [<http://www.teslasociety.com/teslafacil.htm>].
- [7] S. C. Wilks, A. B. Langdon, T. E. Cowan, M. Roth, M. Singh, S. Hatchett, M. H. Key, D. Pennington, A. MacKinnon, and R. A. Snavely, *Phys. Plasmas* **8**, 542 (2001); M. Passoni and M. Lontano, *Phys. Rev. Lett.* **101**, 115001 (2008); M. Passoni, L. Bertagna, and A. Zani, *New. J. Phys.* **12**, 045012 (2010); T. Tajima, J. M. Dawson, *Phys. Rev. Lett.* **43**, 267 (1979); See also: J. Badziak, *Opto-electr. Rev.* **15**, 1 (2007), and references therein.
- [8] T. Esirkepov, M. Borghesi, S. V. Bulanov, G. Mourou, and T. Tajima, *Phys. Rev. Lett.* **92**, 175003 (2004).
- [9] A. Macchi, F. Cattani, T. V. Liseykina, and F. Cornolti, *Phys. Rev. Lett.* **94**, 165003 (2005).
- [10] T. V. Liseykina, M. Borghesi, A. Macchi, and S. Tuveri, *Plasma Phys. Controlled Fusion* **50**, 124033 (2008).

- [11] F. Peano, J. Vieira, L. O. Silva, R. Mulas, and G. Coppa, *New J. Phys.* **10**, 033028 (2008); F. Peano, J. Vieira, R. A. Fonseca, R. Mulas, G. Coppa, and L. O. Silva, *IEEE Trans. Plasma Sci.* **36**, 1857 (2008).
- [12] Y. I. Salamin, Z. Harman, and C. H. Keitel, *Phys. Rev. Lett.* **100**, 155004 (2008).
- [13] I. V. Pogorelsky, V. Yakimenko, M. Polyanskiy, P. Shkolnikov, M. Ispiryan, D. Neely, P. McKenna, D. Carroll, Z. Najmudin, and L. Willingale, *Nucl. Instrum. Methods Phys. Res., Sect. A* **620**, 67 (2010).
- [14] C. A. J. Palmer *et al.* *Phys. Rev. Lett.* **106**, 014801 (2011).
- [15] See [[http://www.gsi.de/portrait/Broschueren/Therapie/synchrotron\(ep2000\).pdf](http://www.gsi.de/portrait/Broschueren/Therapie/synchrotron(ep2000).pdf)].
- [16] Y. I. Salamin, *Appl. Phys. B* **86**, 319 (2007).
- [17] S. Quabis, R. Dorn, M. Eberler, O. Glöckl, and G. Leuchs, *Appl. Phys. B* **72**, 109 (2001).
- [18] R. Dorn, S. Quabis, and G. Leuchs, *Phys. Rev. Lett.* **91**, 233901 (2003).
- [19] S. Quabis, R. Dorn, and G. Leuchs, *Appl. Phys. B* **81**, 597 (2005).
- [20] Y. I. Salamin, *Opt. Lett.* **31**, 2619 (2006); *New J. Phys.* **8**, 133 (2006); **10**, 069801 (2008).
- [21] Y. I. Salamin and C. H. Keitel, *Phys. Rev. Lett.* **88**, 095005 (2002); Y. I. Salamin, G. R. Mocken, and C. H. Keitel, *Phys. Rev. E* **67**, 016501 (2003).
- [22] E. Esarey, P. Sprangle, and J. Krall, *Phys. Rev. E* **52**, 5443 (1995).
- [23] J. D. Lawson, *IEEE Trans. Nucl. Sci.* **NS-26**, 4217 (1979); P. M. Woodward, *J. IEE* **93**, 1554 (1947).
- [24] Y. I. Salamin, *Phys. Rev. A* **82**, 013823 (2010).
- [25] B. Galow, Z. Harman, and C. H. Keitel, *Opt. Express* **18**, 25950 (2010); B. Galow, Y. I. Salamin, T. V. Liseykina, Z. Harman, and C. H. Keitel, *Phys. Rev. Lett.* **107**, 185002 (2011).
- [26] A. Maksimchuk, S. Gu, K. Flippo, D. Umstadter, and V. Y. Bychenkov, *Phys. Rev. Lett.* **84**, 4108 (2000).
- [27] R. A. Snavely *et al.* *Phys. Rev. Lett.* **85**, 2945 (2000).
- [28] S. Karsch, S. Düsterer, H. Schwoerer, F. Ewald, D. Habs, M. Hegelich, G. Pretzler, A. Pukhov, K. Witte, and R. Sauerbrey, *Phys. Rev. Lett.* **91**, 015001 (2003).
- [29] T. E. Cowan *et al.* *Nucl. Instrum. Methods Phys. Res.* **544**, 277 (2005).
- [30] L. Romagnani *et al.* *Phys. Rev. Lett.* **95**, 195001 (2005).
- [31] B. M. Hegelich, B. J. Albright, J. Cobble, K. Flippo, S. Letzring, M. Paffett, H. Ruhl, J. Schreiber, R. K. Schulze, and J. C. Fernández, *Nature (London)* **439**, 441 (2006).
- [32] H. Schwoerer, S. Pfotenhauer, O. Jäkel, K.-U. Amthor, B. Liesfeld, W. Ziegler, R. Sauerbrey, K. W. D. Ledingham, and T. Esirkepov, *Nature (London)* **439**, 445 (2006).
- [33] B. J. Albright, L. Yin, B. M. Hegelich, K. J. Bowers, T. J. T. Kwan, and J. C. Fernández, *Phys. Rev. Lett.* **97**, 115002 (2006).
- [34] M. Roth *et al.* *Opt. Commun.* **264**, 519 (2006).
- [35] [<http://www.extreme-light-infrastructure.eu/pictures/ELI-scientific-case-id17.pdf>].
- [36] [<http://www.hiperlaser.org/docs/tdr/HiPERTDR2.pdf>].
- [37] L. Robson *et al.*, *Nature Physics* **3**, 58 (2007).
- [38] B. Qiao, M. Zepf, M. Borghesi, and M. Geissler, *Phys. Rev. Lett.* **102**, 145002 (2009).
- [39] K. T. McDonald, [<http://www.hep.princeton.edu/mcdonald/accel/gaussian.ps>]; [<http://www.hep.princeton.edu/mcdonald/accel/gaussian2.ps>].